中国激光

光纤耦合周期极化铌酸锂薄膜波导器件的研究

冯新凯[1,2]，陈怀熹[1]，陈家颖[1,2]，梁万国[1*]

[1]中国科学院福建物质结构研究所，福建 福州 350002；

[2]中国科学院大学，北京 100049

摘要　对硅基周期极化铌酸锂(PPLN)薄膜脊形波导进行了理论分析，并使用有限元软件模拟了25 ℃下泵浦波长为1560 nm的PPLN脊形波导的准相位匹配(QPM)周期与波导脊高和脊宽的关系。仿真结果表明，在相同脊宽(10 μm)或脊高(10 μm)下，PPLN脊形波导的QPM周期随着脊高或脊宽的增加而增大，最后趋于常数(即块状PPLN的QPM周期)。进一步模拟了在脊高和脊宽维持不变的情况下，PPLN脊形波导的QPM周期与温度之间的关系。结果表明，随着温度的增加，PPLN脊形波导的QPM周期逐渐减小，并且温度每升高1 ℃，QPM周期减小约3 nm。根据仿真结果制作了硅基片上集成PPLN脊形波导器件，将其封装成小体积的光纤入光纤出的波导，并测试了性能。当温度为24.8 ℃、1560 nm基频光输入功率为1.2 W时，最大输出653 mW的倍频光，光光转换效率达54.4%，归一化转换效率为20.2 %·W^{-1}·cm^{-2}。

关键词　非线性光学；周期极化铌酸锂；薄膜；准相位匹配；脊形波导

中图分类号　O437　　**文献标志码**　A　　**DOI**：10.3788/CJL230448

1　引　　言

周期极化铌酸锂(PPLN)是一种用于激光波长转换的优秀非线性晶体[1]。与通常需要高峰值脉冲功率输入的传统非线性晶体相比，PPLN由于其周期性非临界相位匹配的特性，具有很高的转换效率，适用于连续波(CW)激光波长转换，被广泛应用在连续激光器系统中[2-4]。另外，还可以通过灵活设计PPLN的准相位匹配(QPM)周期，实现全彩色激光[5-7]输出，PPLN具有很强的实用价值。近年来，人们为了提高CW激光器的非线性频率转换效率，注意力逐渐从PPLN体块[8-9]转移到PPLN薄膜光波导[10]。

1998年，Levy等[11]通过离子注入法制备了9 μm厚的铌酸锂(LN)薄膜。2003年，Nishida等[12]利用精密切割技术制备了直接键合PPLN脊形波导。2004年，Rabiei等[13]利用离子注入和键合技术制备了一层680 nm厚的LN薄膜。2010年，Hu等[14]使用离子切片和层转移方法制备了厚度为0.76 μm的3 inch(1 inch=2.54 cm)晶圆级LN单晶薄膜，并受绝缘体上硅(SOI)晶片名称的启发，将其命名为绝缘体铌酸锂(LNOI)。目前，多家供应商可提供尺寸高达6 inch的光学质量LNOI晶片，加速了薄膜化铌酸锂晶体相关器件的开发。国内针对PPLN薄膜光波导器件展开了深入详实的研究[15-17]。基于PPLN波导的非线性频率转换器件在众多领域中得到了广泛的应用，如光学通信[18-19]、量子光学[20]、微波光学[21]和光谱学[22]等。

本文简单介绍了硅基PPLN薄膜脊形波导的基本结构和原理，设计并制作了紧凑型光纤进光纤出PPLN波导封装模块。

2　理论分析

对硅基PPLN薄膜脊形波导(图1)的倍频进行了分析，主要是计算一定结构的波导在基频光λ_1处的二次谐波QPM极化周期Λ_{SHG}，以下简称为QPM周期。对于特定的PPLN脊形波导结构，其基模的有效折射

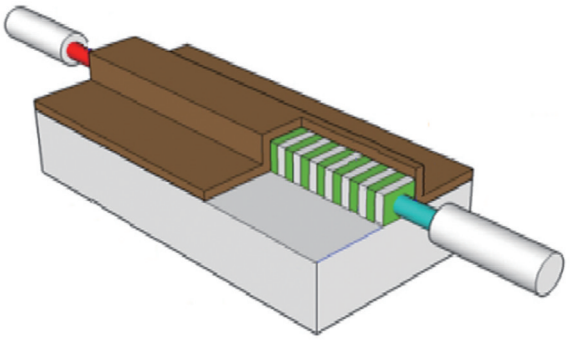

图1　PPLN脊形波导结构示意图

Fig. 1　Structural diagram of PPLN ridge waveguide

收稿日期：2023-01-09；**修回日期**：2023-02-21；**录用日期**：2023-03-15；**网络首发日期**：2023-03-25

基金项目：福建省中科院STS计划配套项目(2022T3012)、中国福建光电信息科学与技术创新实验室(闽都创新实验室)自主部署项目(2021ZZ104)

通信作者：*wgl@fjirsm.ac.cn

率 n_{eff} 是确定的。利用准相位匹配原理[23]，基频光 ω_1 经过 PPLN 脊形波导后获得频率为 $\omega_{\mathrm{SHG}}=2\omega_1$ 的倍频光。由于晶体材料的色散效应[23]，它们的波矢量失配为

$$\Delta k_{\mathrm{SHG}}=k_{\mathrm{SHG}}-2k_1-\frac{2\pi}{\Lambda_{\mathrm{SHG}}},\tag{1}$$

式中：k_{SHG} 为倍频光的波矢量大小；$k_1=2\pi n_1/\lambda_1$ 为对应波长 λ_1 的波矢量大小，其中 n_1 为对应波长 λ_1 的折射率。

当相位失配量 $\Delta k_{\mathrm{SHG}}=0$ 时，即可满足准相位匹配，此时 QPM 周期满足

$$\frac{1}{\Lambda_{\mathrm{SHG}}}=\frac{n_{\mathrm{SHG}}}{\lambda_{\mathrm{SHG}}}-\frac{2n_1}{\lambda_1},\tag{2}$$

化简得

$$\Lambda_{\mathrm{SHG}}=\frac{\lambda_1}{2(n_{\mathrm{SHG}}-n_1)},\tag{3}$$

式中：$\lambda_1=2\lambda_{\mathrm{SHG}}$，其中 λ_{SHG} 为倍频光的波长。

由于铌酸锂晶体是各向异性的双折射材料，因此在设计 PPLN 的 QPM 周期时，要考虑其折射率随波长及温度的变化。铌酸锂晶体的色散特性由 Sellmeier 方程[24]给出

$$n^2=a_1+b_1f+\frac{a_2+b_2f}{\lambda^2-(a_3+b_3f)^2}+\frac{a_4+b_4f}{\lambda^2-a_5^2}-a_6\lambda^2,\tag{4}$$

$$f=(T-T_0)(T+T_0+2\times273.16)=(T-24.5)(T+570.82),\tag{5}$$

式中：n 为铌酸锂晶体的折射率；$a_1\sim a_6$ 和 $b_1\sim b_4$ 为 Sellmeier 系数；f 为与温度有关的参数；λ 为铌酸锂晶体中的光波长；T_0 为室温，这里为 24.5 ℃；T 为晶体的摄氏温度。对于掺杂摩尔分数为 5% 的掺镁铌酸锂晶体，式(5)中的经验系数可在文献[24]中查得。

该 Sellmeier 方程仅适用于铌酸锂块状结构，如果要计算波导结构，需要通过有限元软件建模，计算特定波导结构下对应波长的有效折射率。本文使用有限元软件模拟了室温下基频光波长为 1560 nm 的 PPLN 的 QPM 周期与波导尺寸之间的关系，如图 2 所示。从

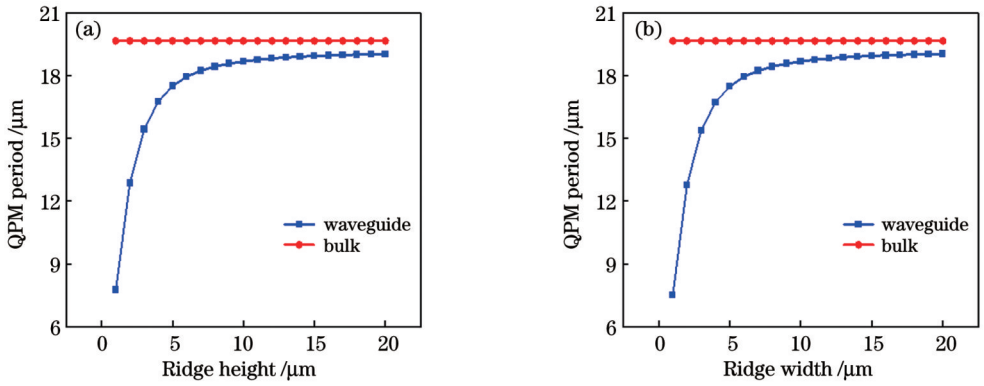

图 2　室温下基频光波长为 1560 nm 的 PPLN 的 QPM 周期与波导尺寸之间的关系。(a)QPM 周期与脊高之间的关系；(b)QPM 周期与脊宽之间的关系

Fig. 2　Relationship between QPM period of PPLN and waveguide size under room temperature when fundamental frequency wavelength is 1560 nm. (a) QPM period versus ridge height; (b) QPM period versus ridge width

图 2(a)可以看出，在同一泵浦波长、同一波导宽度下，PPLN 波导的 QPM 周期随着波导脊高的增加而增大，最后趋于常数，即块状的极化周期。图 2(b)展示了与图 2(a)相似的特性，只是 PPLN 波导的 QPM 周期有微小的差异。为了充分利用 PPLN 的高非线性系数 d_{33}，采用 0 类匹配，即泵浦和二次谐波产生(SHG)信号均采用横磁(TM)偏振。此外，尽管波导可以是多模的，这里也仅考虑基本导模之间的相位匹配。

图 3 给出了基频光波长为 1560 nm 及脊高和脊宽都为 10 μm 的 PPLN 的极化周期与温度之间的关系。可以看出，无论是 PPLN 块状晶体还是脊形波导，在同一基频波长下，QPM 周期均随着温度的增加而逐渐降低；温度每升高 1 ℃，QPM 周期减小 3 nm 左右。

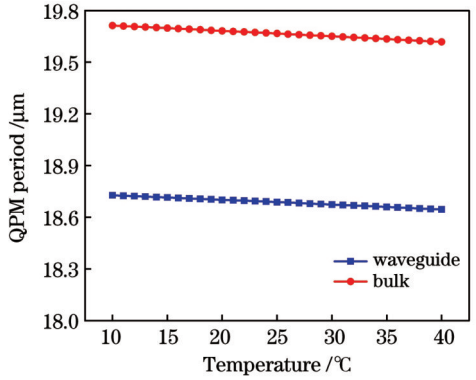

图 3　基频光波长为 1560 nm 及脊高和脊宽都为 10 μm 的 PPLN 的 QPM 周期与温度之间的关系

Fig. 3　QPM period of PPLN versus temperature when fundamental frequency wavelength is 1560 nm and both ridge height and width are 10 μm

3　波导制作与封装

硅基PPLN薄膜脊形波导的制作过程(图4)如下:首先,对一块Z切厚度为0.5 mm的掺杂5%(摩尔分数)MgO的铌酸锂晶片进行高压极化处理。根据上面的分析,极化周期选择为18.7 μm,以获得泵浦波长在1560 nm附近的相位匹配。极化处理完成后,在PPLN晶片的一侧沉积一层约600 nm厚的二氧化硅薄膜缓冲层,然后溅射一层厚度为300 nm左右的金。取另外一块0.5 mm厚精密抛光的硅晶片,镀上一层厚约300 nm的金,并将其与PPLN晶片进行键合。该过程在室温下实现,避免了两个晶圆热膨胀系数的不同而产生的机械应力。接着进行减薄抛光,形成PPLN薄膜。最后利用精密划片机制备所需尺寸的PPLN脊形波导[25],波导的走向为X方向。

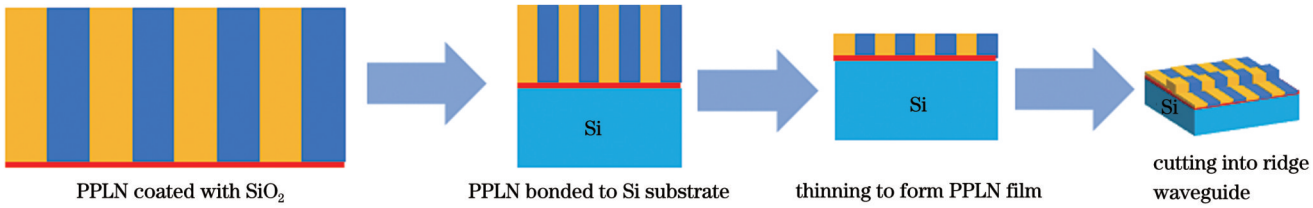

图4　PPLN脊形波导的制备过程

Fig. 4　Preparation process of PPLN ridge waveguide

这里对PPLN薄膜脊形波导的制作工艺进行了改进。例如,选择二氧化硅薄膜的厚度为600 nm,而不是常规的2 μm或者4.7 μm等。2011年,日本NTT公司在Z切的500 μm厚的Mg:LN上溅射一层0.5 μm厚的二氧化硅,并贴在0.5 mm厚的同成分铌酸锂(CLN)基底上,通过机械化学抛光(CMP)方法制作了4 μm厚的LN薄膜,最后测得该脊形波导的传输损耗小于0.5 dB·cm^{-1}@1550 nm[26]。2016年,Chauvet等[27]使用300 nm厚的二氧化硅缓冲层,制作了脊高和脊宽都为10 μm的PPLN脊形波导,测得波导的传输损耗大约为0.8 dB·cm^{-1}。可见600 nm厚的二氧化硅缓冲层不会引起较大的波导损耗。

这里使用的PPLN脊形波导的截面尺寸为10 μm×10 μm,长度为20 mm,使用芯径为8.5 μm、数字孔径(NA)为0.125、模场直径为10.1 μm的单模保偏光纤进行端面直接耦合,封装制作的器件如图5所示。

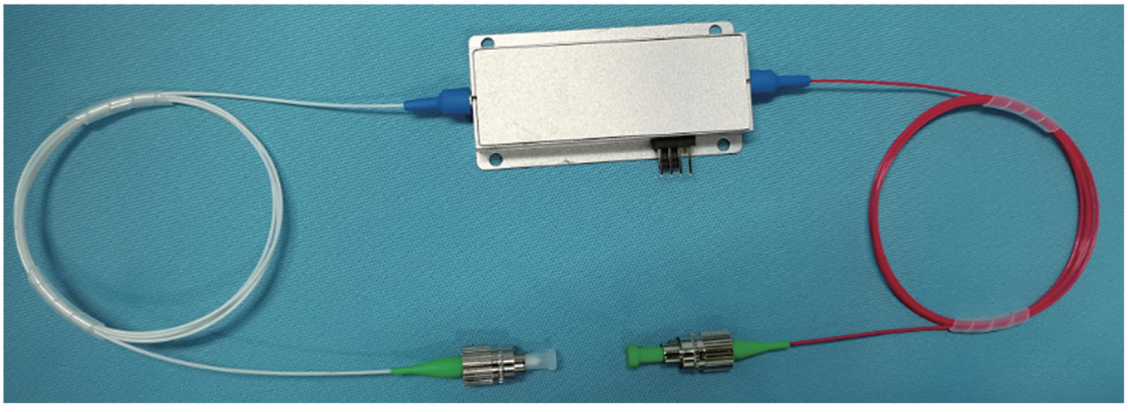

图5　硅基PPLN薄膜脊形波导器件

Fig. 5　Silicon-based PPLN thin film ridge waveguide device

光纤进光纤出PPLN波导封装模块的测试装置图如图6所示,使用可调谐激光光源将波长调整到1560 nm,激光经过窄带掺铒光纤放大器(EDFA)后被输入到PPLN脊形波导中,在输出端加一个1560 nm高反、780 nm高透的滤光片,最后激光进入光功率计。因为PPLN的折射率是温度的函数,因此需要对晶体进行控温。这里使用温控器(精度为0.01 ℃,控温范围是室温到200 ℃)对PPLN波导封装模块进行控温。如图7(a)所示,当温度为24.8 ℃时,模块的输出光波长为780 nm(实验中使用的光谱仪偏差为0.2 nm)。当光纤放大器输出的泵浦功率(P_p^{in})最大为1.6 W时,扣除输入端光纤与波导的耦合损耗后,输入泵浦功率(P_p^0)为1.2 W,波导输出端的耦合泵浦功率(P_p^L,无SHG)为0.9 W,此时输出倍频光的功率是653 mW[图7(b)],光光转换效率为54.4%(P_p^0到SHG功率),归一化转换效率为20.2%·W^{-1}·cm^{-2}(P_p^L到SHG功率)。扣除输入端光纤与波导的耦合损耗后,基于输入泵浦功率P_p^0,计算得到波导的光光转换效率为72.5%,略低于文献[28]的光光转换效率(73%)。

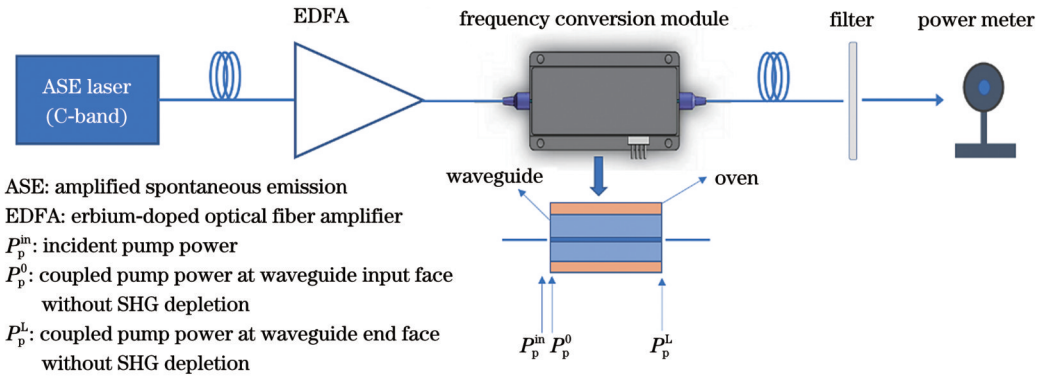

图 6　实验装置图

Fig. 6　Schematic of experimental setup

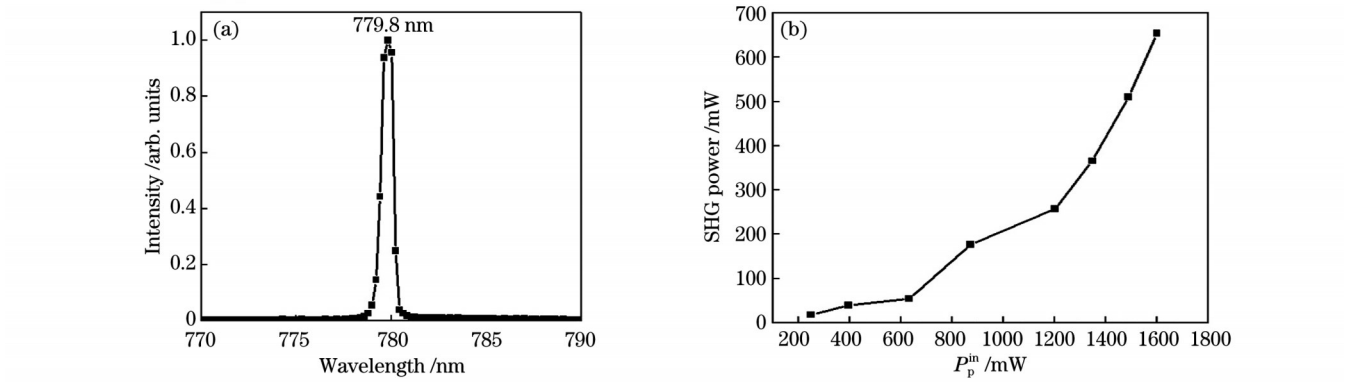

图 7　硅基 PPLN 薄膜脊形波导器件的测试结果。(a)光纤进光纤出 PPLN 波导封装模块的输出光谱图;(b)PPLN 波导封装模块的输出功率与输入功率之间的关系

Fig. 7　Test results of silicon-based PPLN thin-film ridge waveguide device. (a) Output spectrum of fiber-in fiber-out PPLN waveguide package module; (b) relationship between output and input power of PPLN waveguide package module

4　结　　论

模拟分析了 25 ℃下脊高或者脊宽为 10 μm 的 PPLN 脊形波导的 QPM 周期与对应波导脊宽和脊高之间的关系。结果显示,在相同泵浦波长及相同波导脊高和脊宽下,PPLN 波导的 QPM 周期随着波导脊高或者脊宽的增加而增大,最后趋于常数(即块状晶体的周期)。分析了在波导脊高和脊宽不变的情况下,同一基频波长时 PPLN 脊形波导的 QPM 周期与温度之间的关系,发现随着温度的增加,QPM 周期逐渐减小,并且温度每升高 1 ℃,QPM 周期减小约 3 nm。对 PPLN 薄膜脊形波导的制作工艺进行了改进,制作了紧凑型光纤进光纤出的波导封装模块,并测试了其性能。当温度为 24.8 ℃,1560 nm 基频光的输入功率为 1.2 W 时,最大输出 653 mW 的倍频光,光光转换效率达 54.4%,归一化转换效率为 20.2%·W^{-1}·cm^{-2}。

参　考　文　献

[1] 孙军, 郝永鑫, 张玲, 等. 铌酸锂晶体及其应用概述[J]. 人工晶体学报, 2020, 49(6): 947-964.
Sun J, Hao Y X, Zhang L, et al. Brief review of lithium niobate crystal and its applications[J]. Journal of Synthetic Crystals, 2020, 49(6): 947-964.

[2] Song S, Lin H Y, Shi W J, et al. Small yellow-green Nd:YAG/PPMgLN laser module at 561.3 nm[J]. Optik, 2021, 232: 166557.

[3] Fedorova K A, Sokolovskii G S, Khomylev M, et al. Efficient yellow-green light generation at 561 nm by frequency-doubling of a QD-FBG laser diode in a PPLN waveguide[J]. Optics Letters, 2014, 39(23): 6672-6674.

[4] Chen H X, Huang H Z, Cheng J X, et al. Broadband yellow-orange light generation based on a step-chirped PPMgLN ridge waveguide[J]. Optics Express, 2022, 30(18): 32110-32118.

[5] Liu X, Zeng X T, Shi W J, et al. Application of a novel Nd:YAG/PPMgLN laser module speckle-suppressed by multi-mode fibers in an exhibition environment[J]. Photonics, 2022, 9(1): 46.

[6] Zhang B, Xu C Q. Compact, and efficient continues wave intra-cavity frequency doubling Nd:YVO_4/MgO: PPLN 542/543 nm green lasers[J]. Optics & Laser Technology, 2020, 122: 105885.

[7] Hisai Y, Nishida Y, Miyazawa H, et al. Generation of 116 mW output power at 461 nm in a periodically poled lithium niobate waveguide[J]. Japanese Journal of Applied Physics, 2022, 61(2): 020701.

[8] Niu Y R, Yan X, Chen J X, et al. Research progress on periodically poled lithium niobate for nonlinear frequency conversion[J]. Infrared Physics & Technology, 2022, 125: 104243.

[9] Liu J, Duan Y M, Li Z H, et al. Recent progress in nonlinear frequency conversion of optical vortex lasers[J]. Frontiers in Physics, 2022, 10: 865029.

[10] Zhang M, Wang C, Kharel P, et al. Integrated lithium niobate electro-optic modulators: when performance meets scalability[J]. Optica, 2021, 8(5): 652-667.

[11] Levy M, Osgood R M, Liu R, et al. Fabrication of single-crystal

lithium niobate films by crystal ion slicing[J]. Applied Physics Letters, 1998, 73(16): 2293-2295.
[12] Nishida Y, Miyazawa H, Asobe M, et al. Direct-bonded QPM-LN ridge waveguide with high damage resistance at room temperature[J]. Electronics Letters, 2003, 39(7): 609-611.
[13] Rabiei P, Gunter P. Optical and electro-optical properties of submicrometer lithium niobate slab waveguides prepared by crystal ion slicing and wafer bonding[J]. Applied Physics Letters, 2004, 85(20): 4603-4605.
[14] Hu H, Gui L, Ricken R, et al. Towards nonlinear photonic wires in lithium niobate[J]. Proceedings of SPIE, 2010, 7604: 76040R.
[15] Lin J T, Farajollahi S, Fang Z W, et al. Electro-optic tuning of a single-frequency ultranarrow linewidth microdisk laser[J]. Advanced Photonics, 2022, 4(3): 036001.
[16] Zhu Y R, Zhou Y, Wang Z, et al. Electro-optically tunable microdisk laser on Er^{3+}-doped lithium niobate thin film[J]. Chinese Optics Letters, 2022, 20(1): 011303.
[17] 陆延青, 肖敏, 彭茹雯, 等. 人工微结构中的量子、类量子效应及功能集成光子芯片研究进展[J]. 中国基础科学, 2020, 22(1): 11-24.
Lu Y Q, Xiao M, Peng R W, et al. Research advances on quantum and quantum-like effects in artificial microstructures and multi-function integrated photonic chip[J]. China Basic Science, 2020, 22(1): 11-24.
[18] 刘时杰, 郑远林, 陈险峰. 铌酸锂薄膜上的非线性频率变换[J]. 光学学报, 2021, 41(8): 0823013.
Liu S J, Zheng Y L, Chen X F. Nonlinear frequency conversion in lithium niobate thin films[J]. Acta Optica Sinica, 2021, 41(8): 0823013.
[19] 乔玲玲, 汪旻, 伍荣波, 等. 超低损耗铌酸锂光子学[J]. 光学学报, 2021, 41(8): 0823012.
Qiao L L, Wang M, Wu R B, et al. Ultra-low loss lithium niobate photonics[J]. Acta Optica Sinica, 2021, 41(8): 0823012.
[20] 朱效舒, 刘俊, 贺涓子, 等. 超构表面在量子光学中的研究与应用[J]. 光学学报, 2022, 42(3): 0327006.
Zhu X S, Liu J, He J Z, et al. Research and application of metasurfaces in quantum optics[J]. Acta Optica Sinica, 2022, 42(3): 0327006.
[21] 季晓伟, 崔建民, 冯立辉, 等. 基于LNOI的环形谐振腔压力传感器[J]. 激光与光电子学进展, 2022, 59(3): 0323001.
Ji X W, Cui J M, Feng L H, et al. Ring resonator pressure sensor based on LNOI[J]. Laser & Optoelectronics Progress, 2022, 59(3): 0323001.
[22] 郭磊, 陈怀熹, 张新彬, 等. 基于MgO: PPLN啁啾结构和频的宽谱黄-橙激光输出[J]. 激光与光电子学进展, 2020, 57(9): 091901.
Guo L, Chen H X, Zhang X B, et al. Broadband yellow-orange laser output based on chirp structure MgO: PPLN sum-frequency [J]. Laser & Optoelectronics Progress, 2020, 57(9): 091901.
[23] Boyd R W. Nonlinear optics[M]. 4th ed. Amsterdam: Academic Press, 2020.
[24] Gayer O, Sacks Z, Galun E, et al. Temperature and wavelength dependent refractive index equations for MgO-doped congruent and stoichiometric $LiNbO_3$[J]. Applied Physics B, 2008, 91(2): 343-348.
[25] Lin J T, Bo F, Cheng Y, et al. Advances in on-chip photonic devices based on lithium niobate on insulator[J]. Photonics Research, 2020, 8(12): 1910-1936.
[26] Kou R, Kurimura S, Kikuchi K, et al. High-gain, wide-dynamic-range parametric interaction in Mg-doped $LiNbO_3$ quasi-phase-matched adhered ridge waveguide[J]. Optics Express, 2011, 19(12): 11867-11872.
[27] Chauvet M, Henrot F, Bassignot F, et al. High efficiency frequency doubling in fully diced $LiNbO_3$ ridge waveguides on silicon[J]. Journal of Optics, 2016, 18(8): 085503.
[28] Cho C Y, Lai J Y, Hsu C S, et al. Power scaling of continuous-wave second harmonic generation in a MgO: PPLN ridge waveguide and the application to a compact wavelength conversion module[J]. Optics Letters, 2021, 46(12): 2852-2855.

Study of Fiber-Coupled Periodically Poled Lithium Niobate Thin Film Waveguide Devices

Feng Xinkai[1,2], Chen Huaixi[1], Chen Jiaying[1,2], Liang Wanguo[1*]

[1]*Fujian Institute of Research on the Structure of Matter, Chinese Academy of Sciences, Fuzhou* 350002, *Fujiang, China*;
[2]*University of Chinese Academy of Sciences, Beijing* 100049, *China*

Abstract

Objective Periodically poled lithium niobate (PPLN) is an excellent nonlinear crystal for laser wavelength conversion. Conventional nonlinear crystals typically require high peak pulse power input. However, because of its periodic non-critical phase matching characteristics, PPLN has high conversion efficiency. It is extremely suitable for continuous wave (CW) laser wavelength conversion and widely used in CW laser systems. In addition, PPLN can realize full-color laser output by flexibly designing its quasi-phase matching (QPM) period, which has strong practical value. There has recently been a gradual shift from bulk PPLN to PPLN thin-film optical waveguides to improve the nonlinear frequency conversion efficiency of CW lasers. In recent years, many domestic research institutions, such as Nanjing University, East China Normal University, Shandong University, and the Chinese Academy of Sciences, have conducted in-depth detailed research on the preparation and application of PPLN thin film optical waveguide devices. Nonlinear frequency conversion devices based on PPLN waveguides have been used in various applications, such as optical communication, quantum optics, microwave optics, and spectroscopy. As applications continue to grow, new requirements are set for the volume and portability of waveguides. This study briefly introduces the basic structure and principle of a silicon-based PPLN thin film ridge waveguide, and a commercially available compact fiber-in-fiber-out PPLN waveguide package module is designed and fabricated.

Methods The fabrication process of the silicon-based PPLN thin-film ridge waveguide is as follows. First, a *Z*-cut lithium niobate wafer (0.5 mm thick) doped with MgO is poled at high voltage. According to the FDTD software analysis results, the poled period is chosen to be 18.7 μm to obtain phase matching of the pump wavelength near 1560 nm. After poling, a silicon dioxide buffer layer with

a thickness of approximately 600 nm is deposited on one side of the PPLN wafer, subsequently, a gold layer of approximately 300 nm thickness is sputtered. Then, another 0.5-mm thick precision polished silicon wafer is coated with a layer of gold of approximately 300 nm thickness and bonded to the PPLN wafer. This process is realized at room temperature, avoiding mechanical stress caused by the different thermal expansion coefficients of both wafers. Next, thinning and polishing are conducted to form the PPLN film. Finally, the PPLN ridge waveguide with the desired size is prepared based on a precision cutting mechanism. The waveguide direction is X direction (Fig. 4). The PPLN ridge waveguide prepared herein has a cross section of 10 μm×10 μm and a length of 20 mm. A single-mode polarization-holding fiber with a core diameter of 8.5 μm, numerical aperture (NA) of 0.125, and mode field diameter of 10.1 μm is used for end-face direct coupling, and the packaged device is shown in Fig. 5.

Results and Discussions A tunable laser source is used to tune the wavelength to 1560 nm. Subsequently it is incident into the PPLN ridge waveguide through a narrow-band erbium-doped fiber amplifier (EDFA). The light at the output of the waveguide passes through a 1560-nm high reflection and 780-nm high transmission filter and enters the optical power meter (Fig. 6). Because the refractive index of PPLN is a function of temperature, it is necessary to control the crystal temperature. Here, a temperature controller (the accuracy is 0.01 ℃, temperature control range is from room temperature to 200 ℃) is used to control the temperature of the PPLN waveguide package module. As shown in Fig. 7(a), when the temperature is 24.8 ℃, the output wavelength of the module is 780 nm (the deviation of the spectrometer used in the experiment is 0.2 nm). When the pump power $P_{\mathrm{p}}^{\mathrm{in}}$ (shown in Fig. 6) at the output of EDFA reaches 1.6 W, the input pump power P_{p}^{0} is calculated to be 1.2 W after deducting coupling loss between the fiber and waveguide at the input, while the coupling pump power $P_{\mathrm{p}}^{\mathrm{L}}$ [without second harmonic generation (SHG)] at the output of the waveguide is 0.9 W. The power of SHG is 653 mW [Fig. 7(b)], the optical-optical conversion efficiency is 54.4% (P_{p}^{0} to SHG power). The normalized conversion efficiency is 20.2%·W^{-1}·cm^{-2} ($P_{\mathrm{p}}^{\mathrm{L}}$ to SHG power). According to the input pump power P_{p}^{0}, after deducting the coupling loss between the input fiber and the waveguide, the optical-optical conversion efficiency of the waveguide is 72.5%.

Conclusions This study simulate and analyze the relationship between the QPM period of the PPLN ridge waveguide with a ridge height or width of 10 μm at 25 ℃ and the corresponding ridge width or height. The QPM period of the PPLN waveguide increases with the increase of ridge height or width at the same pump wavelength and ridge height or width and finally tends to a constant, that is, the period of bulk PPLN crystal. The relationship between the QPM period and temperature of the PPLN ridge waveguide with constant ridge height and width at the same pump wavelength is analyzed. The QPM period decreases gradually with the increase in temperature, and the QPM period decreases by approximately 3 nm when the temperature rises by 1 ℃. Here, the fabrication process of the PPLN thin-film ridge waveguide is improved. For example, the thickness of the silicon dioxide buffer layer is 600 nm. The waveguide package module with compact fiber in and out is fabricated, and its performance tested. When the temperature is 24.8 ℃ and the input power of 1560 nm pump light is 1.2 W, the maximum power of SHG is 653 mW, the optical-optical conversion efficiency is 54.4%, and the normalized conversion efficiency is 20.2%·W^{-1}·cm^{-2}.

Key words nonlinear optics; periodically poled lithium niobate; thin films; quasi-phase matching; ridge waveguide